Potential Errors in the Application of Thermal-based Energy Balance Models with Coarse Resolution Data

William P. Kustas*[a], Nurit Agam [a], Martha C. Anderson [a], Fuqin Li [a], Paul D. Colaizzi [b]
[a] USDA-ARS Hydrology & Remote Sensing Lab., B007, BARC-W, Beltsville, MD, USA 20705;
[b] USDA-ARS Conservation & Production Research Lab., Bushland, TX, USA 79012

ABSTRACT

A thermal sharpening algorithm (TsHARP) providing fine resolution land surface temperature (LST) to the Two-Source-Model (TSM) for mapping evapotranspiration (ET) was applied over two agricultural regions in the U.S. One site is a rainfed corn and soybean production region in central Iowa, while the other is an irrigated agricultural area in the Texas High Plains. Application of TsHARP to coarse (1 km) resolution thermal data over the rainfed agricultural area is found to produce reliable fine/within-field (60 m) resolution ET estimates, while in contrast, the TsHARP algorithm applied to the irrigated area does not perform as well, possibly due to significant sub-pixel moisture variations from irrigation. As a result, there may be little benefit in applying TsHARP for generating TSM-derived 60 m ET maps for the irrigated compared to the rainfed region. Consequently, reliable estimation of fine/within-field ET and crop stress still requires fine native resolution thermal imagery in areas with significant sub-pixel moisture variations.

Keywords: thermal remote sensing, two-source model, surface energy balance, evapotranspiration, crop stress, rainfed and irrigated agriculture

1. INTRODUCTION

Over the past several decades, methods for deriving spatially-distributed evapotranspiration (ET) maps have been developed by applying visible–near-infrared (VIS/NIR) and the thermal infrared (TIR) imagery with surface energy balance models[1]. The spatial resolution of the resulting ET maps is determined by the pixel resolution of the TIR sensor which are 2-10 time coarser than the co-located VIS/NIR sensors. For water resource and crop monitoring, ideally ET maps would be available on daily basis at fine spatial resolutions (< 100 m). However, a trade-off exists between the spatial and temporal resolutions of current satellite sensor systems, where they either have high-spatial/low-temporal or low-spatial/high-temporal resolution.

A compromise in the spatial and temporal resolution requirement has come from using Moderate Resolution Imaging Spectrometer (MODIS) on board the Terra/Aqua satellites where~1 km ET maps can be generated every few days[2]. While providing reasonable temporal coverage, ~ 1 km resolution ET does not provide any information on within-field variations, and often the pixel will be comprised of different crops. To address this shortcoming, another strategy utilizes the functional relationship between VIS/NIR and TIR to sharpen the 1-km MODIS TIR imagery to the resolution of the MODIS VIS/NIR bands (250m) and hence derive near-daily ET maps at spatial resolutions that resolve typical individual field sizes (TsHARP[3,4]). Within-field ET could be estimated if finer resolution VIS/NIR data were available close in time (days) to the MODIS overpass, say from Landsat or ASTER. Provided that the sharpening algorithm can satisfactorily reproduce the actual LST distributions at the finer targeted resolutions, this approach may provide the most viable option for deriving routine remotely-sensed ET maps at field and sub-field scale.

The utility of applying the TsHARP algorithm for fine resolution ET estimation using the TSM was examined over two agricultural regions in the U.S.: a rainfed corn and soybean production region in the Walnut Creek Watershed in central Iowa, and an irrigated agricultural area in the Texas High Plains within the Texas Panhandle. A comparative analysis of performance of the TsHARP/TSM framework for computing fine scale ET in these two representative areas is presented.

*Bill.Kustas@ars.usda.gov; phone 1 301 504-7490; fax 1 301 504-8931; www.ars.usda.gov

Remote Sensing for Agriculture, Ecosystems, and Hydrology IX, edited by Christopher M. U. Neale, Manfred Owe, Guido D'Urso, Proc. of SPIE Vol. 6742, 674208, (2007) · 0277-786X/07/$18 · doi: 10.1117/12.737776

2. METHODOLOGY

2.1 Two-Source Model (TSM) formulation

Details of the formulations currently used in TSM is described elsewhere[5,6]. In the TSM, the key remotely sensed variable is directional radiometric surface temperature, $T_R(\theta)$, obtained from TIR observations at zenith view angle θ. For a partially vegetated patch of land, it is assumed that $T_R(\theta)$ is a composite of the characteristic canopy and soil temperatures, T_C and T_S, weighted by the fractional vegetation cover $f_C(\theta)$ apparent at angle θ:

$$T_R(\theta) \approx [f_C(\theta)T_C^4 + (1 - f_C(\theta))T_S^4]^{1/4}. \quad (1)$$

The sensible heat flux (H) is partitioned between the vegetated canopy (H_C) and soil (H_S) using the following relations:

$$H = H_C + H_S = \rho C_P \frac{T_{AC} - T_A}{r_A} \quad (2)$$

$$H_C = \rho C_P \frac{T_C - T_{AC}}{r_X} \quad (3)$$

$$H_S = \rho C_P \frac{T_S - T_{AC}}{r_S} \quad (4)$$

where ρC_P is the volumetric heat capacity of air ($Jm^{-3}K^{-1}$), T_{AC} is the air temperature in canopy-air space, T_A is the air temperature, r_A is the aerodynamic resistance to heat transfer across the canopy-surface layer interface, r_X is the total boundary layer resistance of the complete canopy of leaves, and r_S is the resistance to heat flow in the boundary layer immediately above the soil surface.

The latent heat flux from the vegetated canopy (LE_C) is initially derived from the Priestley-Taylor formula[7]

$$LE_C = \alpha_{PT} f_G \frac{\Delta}{\Delta + \gamma} Rn_C \quad (5)$$

where γ is the psychrometric constant (≈67 PaK^{-1}), α_{PT} is Priestley-Taylor parameter (~ 1.3), f_G is the fraction of the leaf area index (LAI) that is green, Δ is the slope of the saturation vapor pressure verses temperature curve, and Rn_C is divergence of net radiation within the vegetative canopy layer. By combining Eq. (5) with Eq. (3) and imposing energy conservation (balance) for the canopy ($Rn_C=LE_C+H_C$), an initial solution for the canopy component and a value for T_{AC} is derived.

With the surface soil heat flux (G) estimated as a fraction of net radiation reaching soil surface, Rn_S

$$G = C_G Rn_S \quad (6)$$

where C_G ~0.35 (expressed as a function of time to accommodate known temporal variation in this "constant"), and imposing energy conservation (balance) for soil ($Rn_S=LE_S+H_S+G$), H_S computed from Eq. (4) using T_{AC} derived in iteration with the canopy equations, and the soil latent heat flux, LE_S, is solved by residual. If LE_S is negative (condensation onto the soil), which is unlikely during daytime convective conditions, this is interpreted as a signature of vegetation stress and LE_c is throttled back from its potential rate given by the Priestley-Taylor approximation (Eq. 5).

The TsHARP algorithm has been utilized to retrieve high-resolution ET maps over experimental sites in the Southern Great Plains (SGP)[8] . TsHARP was recently refined in an application over the upper Midwest corn and soybean production region in central Iowa during the growing season of 2002[4]. The basic algorithm exploits the natural covariation that typically exists between surface temperature and vegetation cover amount. Where evaporative fluxes are not energy limited, areas with higher vegetation cover tend to have lower surface temperature due to cooling by transpiration. Bare, dry soil is generally hotter than is healthy transpiring vegetation. It is assumed that this covariation exists within a sensor scene at multiple spatial resolutions.

2.2 Thermal sharpening algorithm, TsHARP

The sharpening procedure uses a simplified form of fractional vegetation cover (f_CS, Eq. 7) derived from the fractional cover-NDVI relationship setting the NDVI scaling coefficients $NDVI_{max}$ and $NDVI_{min}$ to 1 and 0, respectively[4]:

$$f_C s = 1 - \left(1 - NDVI\right)^{0.625} \tag{7}$$

A least-squares regression is performed between T_R and f_Cs, after NDVI has been aggregated to the coarser thermal resolution ($NDVI_{low}$):

$$\hat{T}_R\left(NDVI_{low}\right) = a_0 + a_1 f_C s_{low} = a'_0 - a'_1\left(1 - NDVI_{low}\right)^{0.625} \tag{8}$$

Here the "hat" symbol indicates a temperature value predicted using the NDVI regression equation. This regression relationship is then applied to the NDVI data at their finer, native resolution ($NDVI_{high}$):

$$\hat{T}_R\left(NDVI_{high}\right) = a'_0 - a'_1\left(1 - NDVI_{high}\right)^{0.625} \tag{9}$$

Errors in the least-squares regression, due to forces driving surface temperatures other than vegetation cover amount (e.g., soil moisture), can be assessed at the coarse scale:

$$\Delta\hat{T}_{R\ low} = T_{R\ low} - \hat{T}_R\left(NDVI_{low}\right) \tag{10}$$

The coarse-scale residual field is added back into the sharpened map such that the original temperature field is recovered through re-aggregation. The sharpened sub-pixel temperatures within each coarse pixel are therefore computed via:

$$\hat{T}_{R\ high} = \hat{T}_R\left(NDVI_{high}\right) + \Delta\hat{T}_{R\ low} \tag{11}$$

where the first term of the right-hand side is evaluated using Eq. (9), and the second residual term from Eq. (10) is constant over the coarse pixel area.

This procedure requires that a range of surface temperature and vegetation cover fraction be present within the image scene, in order to develop a significant regression relationship. TsHARP therefore does not perform well over scenes in which there is little variability in surface temperature; for example during nighttime or early morning, or in areas where surface conditions are relatively homogeneous. However, the practical benefits of sharpening such scenes are limited. Homogeneous scenes will not profit from sharpening, and most remote-sensing based energy balance models are applied mid-morning and mid-afternoon – times when TsHARP would be most useful and applicable

3. DATA

3.1 Site and satellite scene description

A grid-box ~10 km north-south by 30 km east-west, encompassing the Walnut Creek Watershed (WCW; centered at 34° 44` N 101° 37` W) was subset from a Landsat ETM+ scene acquired on July 1, 2002. The WCW lies within the upper Midwest corn and soybean production region in central Iowa, characterized mainly by rainfed agriculture. This area is representative of ~60% of the US cultivated cropland. In this humid region, the most rapid growth in corn and soybean crops is observed in June-July. During this period, rainfall events are often in the form of thunderstorms, providing brief and intense showers. The July 1 scene was acquired following a ~10 day dry-down interval, resulting in strong variability in soil moisture and crop conditions.

A subset was extracted from the Texas High Plains (THP) region (~10 km north-south by 30 km east-west, centered at 34° 37' N, 102° 53' W) lying within a full Landsat ETM+ scene (acquired on September 22, 2002) which encompassed the northern part of the Texas-New-Mexico state border. This area is part of the Southern High Plains, within the larger Great Plains of the western United States, and is mostly comprised of irrigated agricultural fields. In the THP region,

September is a relatively dry month, during which the cotton crops are reaching maturity and are thus unlikely to be irrigated, while emerging winter wheat crops are typically receiving irrigation. The studied scene was therefore comprised of a large variability in vegetation cover and moisture conditions (due to irrigation) over the study area.

3.2 Image Processing

The two Landsat ETM+ scenes provided VIS/NIR and TIR data at 30 and 60 m native resolution, respectively. The scenes were atmospherically corrected using MODTRAN. The brightness temperatures were then corrected for emissivity effects using a fractional cover mixture model to retrieve surface radiometric temperature[9] .

3.3 Scaled Inputs

Three spatial resolutions were examined in this study: 60 and 240 (hereafter referred to as "finer resolutions"), and 960 m (hereafter referred to as "coarse resolution"). In order to avoid errors introduced by inter-sensor comparisons caused by differences in view angle, pixel registration, and overpass time, the Landsat ETM+ VIS/NIR and TIR bands were spatially aggregated to simulate MODIS-resolution data, sharpened, and then validated with respect to ETM+ TIR distributions at the finer resolutions. Note that unless explicitly mentioned, the described processes were applied similarly to both sites.

During the Soil Moisture Atmosphere Coupling Experiment (SMACEX) over the WCW extensive sampling of vegetation cover fraction and canopy architecture was conducted, and a supervised land-cover classification was performed using multi-temporal Landsat imagery [10] . Due to a lack of ground-truth data over the THP, a landuse map for the Texas scene was obtained by classifying the study area into general land cover categories of agricultural land and natural vegetation using a semi-unsupervised classification technique applied to 5 VIS/NIR Landsat ETM+ scenes collected in 2002.

Fraction vegetation cover and canopy height, which are the main parameters derived from the NDVI data (hereafter the VI parameters), were determined at the target resolutions (60, and 240 m) using the aggregated NDVI maps, while maintaining high-resolution (30 m) information derived from the landuse maps. Accordingly, the derived fluxes represent outputs one might obtain in practice, using 30 m landuse maps in conjunction with NDVI data available at the target resolution.

Simulated TIR images at 240 and 960m resolutions were generated by converting the original brightness temperature data at 60 m to radiance values using the Stephan-Boltzmann law, computing an average radiance over the coarser pixel area, and then re-converting to brightness temperature. The sharpening algorithm was then applied to the coarse 960 m TIR field to create sharpened temperature fields at each of the finer resolutions.

For both sites, meteorological data used by the TSM, consisting primarily of 30-min average wind speed, air temperature, relative humidity, and solar radiation were obtained from local weather stations and applied uniformly across the images. The observations were collected ~2 m above the canopy layer.

For each of the sharpening target resolutions (60 and 240m), three different types of flux maps have been generated and intercompared:

— *Reference* — The original 60 m TIR data were used in conjunction with the VI parameters at 60 m to derive 60 m flux maps and then aggregated to 240 and 960 m. These maps were used as a reference to which the other methods were compared.

— *TsHARP* — The coarse (960 m) temperature field was sharpened to 60 and 240 m using the above described sharpening algorithm (section 2.2). The TSM was executed at these two finer TIR resolutions to create flux maps at 60 and 240 m.

— *uniFlux* — The coarse resolution TIR data were utilized by the TSM to generate 960 m flux maps. These coarse resolution fluxes were then uniformly resampled to the finer resolution grids to create flux maps at 60 and 240 m. These maps serve as a baseline for assessing the improvement in spatial information content achieved by sharpening the input thermal imagery.

4. RESULTS AND DISCUSSION

The TsHARP algorithm has been applied to 1-km TIR imagery for the WCW and THP regions[4,11]. Table 1 provides difference statistics with the reference T_R (quantified by mean absolute error, MAE) assessing the utility of the sharpening algorithm in retrieving finer resolutions TIR over these two sites. The utility of TsHARP is assessed by comparing MAE values with those obtained from uniformly resampling the coarse resolution T_R to the finer resolution, referred to as uniLST (similar to uniFlux approach). Note a greater relative reduction in the MAE value (between uniLST and TsHARP) is observed for the WCW versus THP site.

Table 1. Difference statistics (MAE values) with the reference T_R using TsHARP and uniLST estimated T_R at the finer pixel (60 and 240 m) resolutions for the WCW (Walnut Creek Watershed-rainfed agriculture) and THP (Texas High Plains-irrigated agriculture)

Site/Approach	MAE of T_R at 60 m (^{o}C)	MAE of T_R at 240 m (^{o}C)
WCW/TsHARP	1.63	1.05
WCW/uniLST	2.22	1.72
THP/TsHARP	1.44	1.07
THP/uniLST	1.82	1.53

A map of the reference T_R at 60 m resolution, the starting course resolution (960 m) T_R and the sharpened T_R at 60 m is illustrated for the WCW and THP study areas in Figure 1. While the TsHARP algorithm does reproduce a finer resolution map that resembles the subfield reference T_R variability, there are areas where the sharpening does poorly, particularly for the THP study area at the extremes (i.e., the very hot and cool pixels)[11].

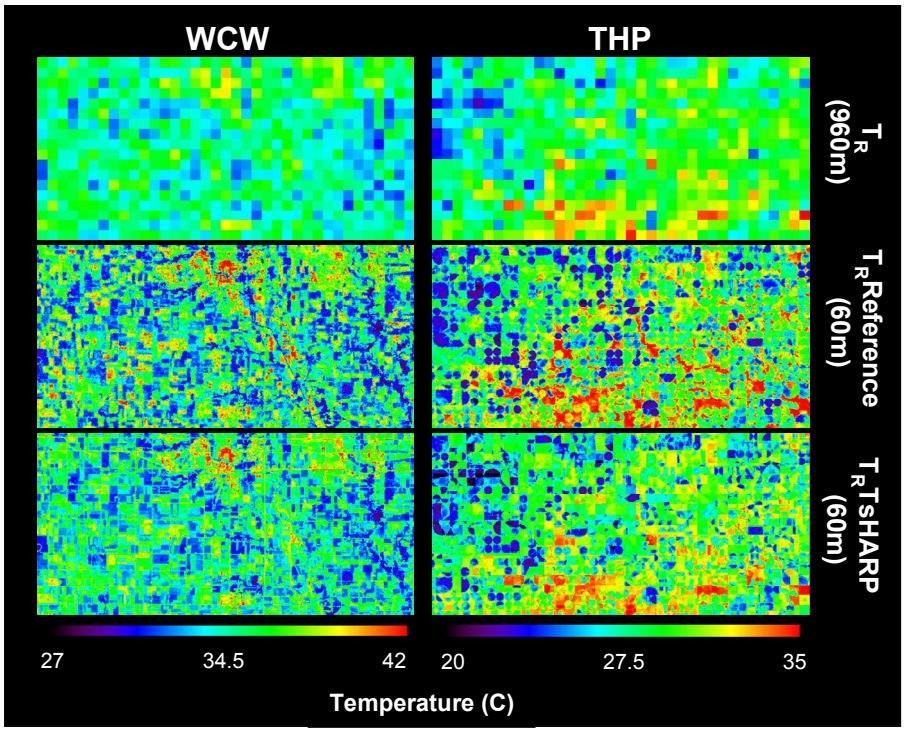

Fig. 1. LST (T_R) maps at 960 m and 60 m spatial resolution from the reference (native resolution), and derived from TsHARP for the (Walnut Creek Watershed-rainfed agriculture) and THP (Texas High Plains-irrigated agriculture).

The use of TsHARP-derived TIR inputs to the TSM in estimating fine resolution *LE* produced inconsistent results between the two sites (Table 2). For the THP, the finer resolution TIR from TsHARP only marginally improved TSM-derived *LE* compared to the uniFlux approach. However, applying TsHARP over the WCW region reduced errors in *LE* estimation at the finer resolutions by 30-60%. Note that relative errors (i.e., MAE/<*LE*>, where < > =scene average) are higher for the THP region (i.e., ~20% versus ~10%) since <LE> ~ 400 W m^{-2} for WCW versus ~150 W m^{-2} for THP.

Table 2. Difference statistics (MAE values) with the reference flux using uniFlux and TsHARP estimated T_R as input to the TSM for estimating *LE* (ET) at the finer pixel (60 and 240 m) resolutions for WCW and THP study sites

Site/Approach	**MAE of *LE* at 60 m (W m^{-2})**	**MAE of *LE* at 240 m (W m^{-2})**
WCW/TsHARP	32	21
WCW/uniFlux	61	48
THP/TsHARP	31	21
THP/uniFlux	34	26

Qualitatively, the difference in the performance of TsHARP in terms of flux evaluations over these two agricultural regions can be seen in the maps of *LE* (ET) at 60m resolution shown in Figure 2. The sharpened thermal images are better able to reproduce the full range in ET present in the reference field for the WCW site than for the THP site. In addition, the THP flux maps suffer from the same "box-like" features in the sharpened TIR images over this site[11]. These boxes demarcate the borders of the coarse (960 m) resolution TIR pixels, and are associated with the reintroduction of the residuals to the TIR-VI sharpening relationship determined at the coarse scale, which are currently distributed uniformly over the coarse pixel area. Future work will identify algorithms for generating non-uniform residual distributions, reducing this effect to some degree. In contrast, these coarse-scale artifacts were not evident in the sharpened TIR fields for WCW, nor do they appear in the derived ET maps[4].

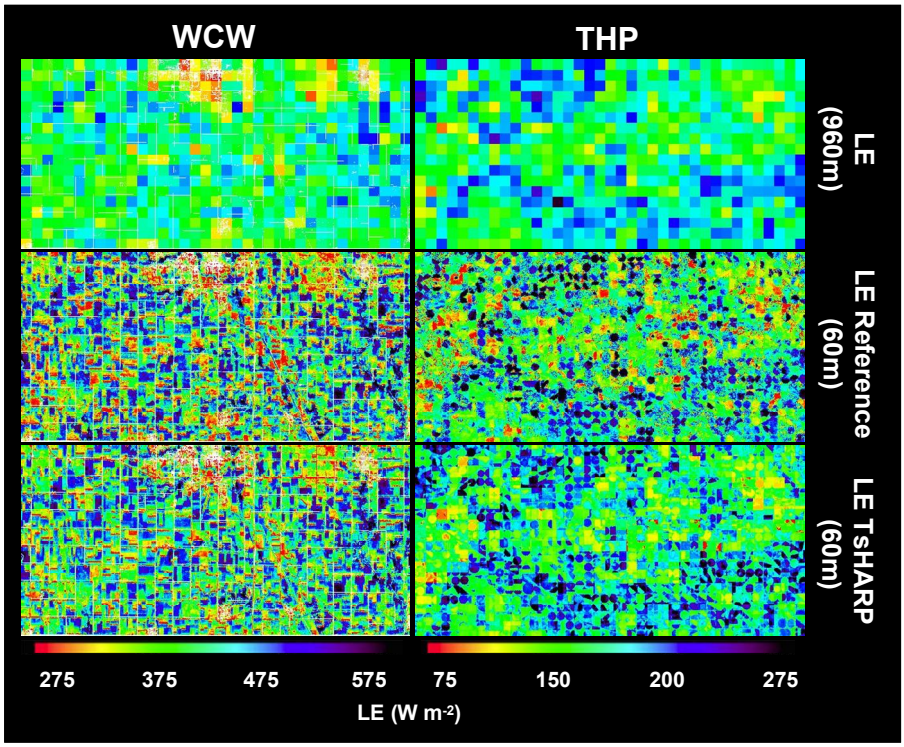

Fig 2. Latent heat flux (LE) maps at 60 m spatial resolution derived by the TSM, using the reference, TsHARP, and uniFlux methods, for the WCW and THP sites. The white areas in the WCW maps mask urban/road pixels having no output.

5. CONCLUSIONS

In the absence of satellite systems providing fine resolution (<100m) thermal satellite data with frequent (every few days) revisit times, TsHARP provides an important tool for monitoring ET at field scales over rainfed agricultural areas. In contrast, over irrigated agricultural regions, TIR data sharpened from 1km resolution and used by the TSM are unable to produce more accurate high resolution ET maps than simply uniformly resampling the 1 km output to finer resolutions. This is likely due to sub-pixel variability in moisture patterns from recent irrigation that are not captured by the thermal sharpening algorithm[12]. Consequently, for precision management and decision support systems designed for irrigated agricultural areas, there is still a need for high resolution (< 100 m) thermal imagery in order to provide important field-scale crop water use information.

ACKNOWLEDGMENTS

This research was supported by Vaadia-BARD Postdoctoral Fellowship Award No. FI-371-2005 from BARD, The United States - Israel Binational Agricultural Research and Development Fund.

REFERENCES

1. Diak, G. R., J. R. Mecikalski, M. C. Anderson, J. M. Norman, W. P. Kustas, R. D. Torn, and R. L. DeWolf, "Estimating land-surface energy budgets from space: Review and current efforts at the University of Wisconsin-Madison and USDA-ARS," *Bull. Amer. Meteorol. Soc*, 85, 65-78 (2004).
2. Nishida, K., R. R. Nemani, J. M. Glassy, and S. W. Running, "Development of an evapotranspiration index from Aqua/MODIS for monitoring surface moisture status," *IEEE Trans. Geosci. Remote. Sens.* 41, 493-501 (2003).
3. Kustas, W. P., J. M. Norman, M. C. Anderson, and A. N. French, "Estimating subpixel surface temperatures and energy fluxes from the vegetation index-radiometric temperature relationship," *Rem. Sen. Environ.* 85, 429-440 (2003).
4. Agam, N., W. P. Kustas, M. C. Anderson, F. Li, and C. M. U. Neale, "A vegetation index based technique for spatial sharpening of thermal imagery," *Rem. Sen. Environ.* 107, 545-558 (2007).
5. Kustas, W. P., and J. M. Norman, "A two-source energy balance approach using directional radiometric temperature observations for sparse canopy covered surfaces", *Agron. J*, 92, 847-854 (2000).
6. Kustas, W.P., J.M. Norman, T.J. Schmugge, T. J., and M.C. Anderson,, "Mapping surface energy fluxes with radiometric temperature". Chapter 7 in: *Thermal Remote Sensing in Land Surface Processes* (Editors D. Quattrochi and J. Luvall), pp. 205-253. CRC Press Boca Raton, Florida, USA (2004).
7. Priestley, C.H.B., and R.J. Taylor, "On the assessment of surface heat flux and evaporation using large-scale parameters," *Monthly Weather Rev.* 100, 81-92 (1972).
8. Anderson, M.C., J.M. Norman, J.R. Mecikalski, R.D. Torn, W.P. Kustas and J.B. Basara, "A Multiscale remote sensing model for disaggregating regional fluxes to micrometeorological scales, *J. Hydromet.* 5, 343-363 (2004).
9. Li, F., T. J. Jackson, W. P. Kustas, T. J. Schmugge, A. N. French, M. Cosh, and R. Bindlish, "Deriving land surface temperature from Landsat 5 and 7 during SMEX02/SMACEX," *Rem. Sen. Environ.* 92, 521-534 (2004).
10. Kustas, W.P., J.L. Hatfield and J.H. Prueger, "The Soil Moisture Atmosphere Coupling Experiment (SMACEX): Background, hydrometeorlogical conditions and preliminary findings," *J. Hydromet.* 6, 791-804 (2005).
11. Agam, N., W. P. Kustas, M. C. Anderson, F. Li, and P. D. Colaizzi, "Utility of thermal sharpening over Texas High Plains irrigated agricultural fields," *J. Geophys. Res – Atmos.* in press.
12. Agam, N., W. P. Kustas, M. C. Anderson, F. Li, and P. D. Colaizzi, "Utility of thermal image sharpening for monitoring field-scale evapotranspiration over rainfed and irrigated agricultural regions," *Geophys. Res. Lett*., in review.